



# Sensitivity of $\beta$ -decay rates to the radial dependence of the nucleon effective mass

A. P. Severyukhin, J. Margueron, I. N. Borzov, Nguyen van Giai

## ► To cite this version:

A. P. Severyukhin, J. Margueron, I. N. Borzov, Nguyen van Giai. Sensitivity of  $\beta$ -decay rates to the radial dependence of the nucleon effective mass. *Physical Review C*, 2015, 91 (034322), <http://journals.aps.org/prc/abstract/10.1103/PhysRevC.91.034322>. 10.1103/PhysRevC.91.034322 . in2p3-01155290

**HAL Id: in2p3-01155290**

**<https://hal.in2p3.fr/in2p3-01155290>**

Submitted on 26 May 2015

**HAL** is a multi-disciplinary open access archive for the deposit and dissemination of scientific research documents, whether they are published or not. The documents may come from teaching and research institutions in France or abroad, or from public or private research centers.

L'archive ouverte pluridisciplinaire **HAL**, est destinée au dépôt et à la diffusion de documents scientifiques de niveau recherche, publiés ou non, émanant des établissements d'enseignement et de recherche français ou étrangers, des laboratoires publics ou privés.

# Sensitivity of $\beta$ -decay rates to the radial dependence of the nucleon effective mass

A. P. Severyukhin,<sup>1</sup> J. Margueron,<sup>2</sup> I. N. Borzov,<sup>1</sup> and N. Van Giai<sup>3</sup>

<sup>1</sup>*Bogoliubov Laboratory of Theoretical Physics, Joint Institute for Nuclear Research, 141980 Dubna, Moscow region, Russia*

<sup>2</sup>*Institut de Physique Nucléaire de Lyon, Université Claude Bernard Lyon 1,*

*IN2P3-CNRS, F-69622 Villeurbanne*

<sup>3</sup>*Institut de Physique Nucléaire, CNRS-IN2P3 and Univ. Paris-Sud, 91405 Orsay, France*

(Dated: May 26, 2015)

We analyze the sensitivity of  $\beta$ -decay rates in  $^{78}\text{Ni}$  and  $^{100,132}\text{Sn}$  to a correction term in Skyrme energy-density functionals (EDF) which modifies the radial shape of the nucleon effective mass. This correction is added on top of several Skyrme parametrizations which are selected from their effective mass properties and predictions about the stability properties of  $^{132}\text{Sn}$ . The impact of the correction on high-energy collective modes is shown to be moderate. From the comparison of the effects induced by the surface-peaked effective mass in the three doubly magic nuclei, it is found that  $^{132}\text{Sn}$  is largely impacted by the correction, while  $^{78}\text{Ni}$  and  $^{100}\text{Sn}$  are only moderately affected. We conclude that  $\beta$ -decay rates in these nuclei can be used as a test of different parts of the nuclear EDF:  $^{78}\text{Ni}$  and  $^{100}\text{Sn}$  are mostly sensitive to the particle-hole interaction through the  $B(\text{GT})$  values, while  $^{132}\text{Sn}$  is sensitive to the radial shape of the effective mass. Possible improvements of these different parts could therefore be better constrained in the future.

PACS numbers: 23.40.-s, 26.30.-k, 21.10.Re

## I. INTRODUCTION

Weak processes such as  $\beta$ -decay rates, electron capture, neutrino scattering and absorption play an important role during the late evolution of massive stars [1]. They are largely responsible for the electron fraction in the core during the core-collapse phase and they continue to play a determinant role in the nuclear synthesis  $r$ -process [2]. Because of their great importance in astrophysical applications, weak processes were extensively investigated within various approaches. The large-scale shell model Monte Carlo (SMMC) method was, for instance, applied to compute  $\beta^\pm$  decay rates for stellar conditions for more than 100 nuclei in the mass range  $A = 45\text{--}65$  [3, 4]. Recently, mean-field based models have been used for the prediction of electron-capture cross sections and rates. Finite-temperature charge-exchange RPA (CERPA) models based on Skyrme or relativistic functionals have been applied to predict electron-capture cross sections using different interactions [5–7]. Mean-field predictions around the Fermi energy are, however, known to suffer from their underestimation of the density of states. In this work, we explore a small correction to the mean field models which increases the density of states around the Fermi energy [8]. Here, we compare the predictions of this model to known experimental values such as  $\beta$  half-lives or collective modes, as a first step before using it for astrophysical applications.

Since the pioneering work of Brown et al. [9] it is known that the level density around the Fermi energy in stable nuclei indicates that the in-medium nucleon effective mass is close to the bare mass. The description of giant resonances such as the giant dipole resonance requires, on the other hand, that the nucleon effective mass in the nuclear medium should be reduced as compared to its value in vacuum [10]. Analysis of the momentum dependence

of the nuclear optical potential also favors an in-medium effective mass lower than in vacuum [11, 12].

These apparently diverging properties of the in-medium effective mass  $m^*$  can be reconciled by considering the two contributions to  $m^*$ : the  $k$ -mass which is also called the non-locality mass, and the  $\omega$ -mass which is induced by dynamical correlations such as particle-phonon coupling [13–17]. The coupling of the collective modes to the single-particle (s.p.) motion is, however, difficult to perform in a self-consistent approach. One of the main problems is coming from the fragmentation of s.p. strength which increases exponentially at each iteration of the self-consistent method. It has therefore been tried to include these correlation directly in the mean field, either at the level of the interaction with density-dependent gradient terms [18], or, loosing the relation with an interaction, at the level of the nuclear energy density functional (EDF) so as to produce a surface-peaked effective mass (SPEM) which, at the same time, does not strongly modify the mean-field [8]. In this study, we will explore the second approach.

Predictions of  $\beta$ -decay rates throughout the nuclear chart within a consistent microscopic nuclear model are difficult. Tuning of models according to the system under study is usually performed, and the description of  $\beta$ -decay rates through a unique microscopic nuclear model does not exist. Since  $\beta$ -decay rates are known to depend strongly on the fine structure around the Fermi level, the difficulties to have a general description could be related to the common issue with mean-field models that the s.p. level density around the Fermi level is too low. The increase of the level density, by using for instance a model producing a SPEM could, in principle, lead to a better description of  $\beta$ -decay rates throughout the nuclear chart.

In microscopic approaches, calculations of nuclear  $\beta$

-decay rates are rather complex. Due to phase-space amplification effects, the calculated  $\beta$ -decay rates are sensitive to both nuclear binding energies and  $\beta$ -strength functions. In an appropriate  $\beta$ -decay model, the correct amount of the integral  $\beta$ -strength should be placed within the properly calculated  $Q_\beta$ -window provided that the spectral distribution is also close to the "true"  $\beta$ -strength function. Furthermore, for consistency the model has to yield correct positions and strengths of the Gamow-Teller (GT) and first-forbidden resonances in the continuum [19]. Another complication is related with the large-scale predictions of nuclear  $\beta$ -decay rates. Such a program is a compromise between accurate results and the necessity to cover extended regions of the nuclear chart including deformed nuclei or even the region with triple prolate-oblate-spherical shape coexistence scenario. In this work, we shall consider only the case of spherical nuclei. A plausible way to detect a change of the  $\beta$ -decay strength function profile due to higher-order corrections could be the analysis of the integral characteristics of  $\beta$ -decay. The half-life is one of such characteristics, being sensitive enough to the  $\beta$ -strength distribution [19]. It is worth to analyze first the doubly-magic  $\beta^\pm$ -unstable nuclides, such as  $^{100,132}\text{Sn}$ , since one can use the simpler CERPA model. Also, we compare to the most neutron-rich ( $(N-Z)/A = 0.28$ ) doubly-magic nucleus  $^{78}\text{Ni}$  which is an important waiting point in the r-process [20]. The next step would then be to study the delayed neutron and especially delayed multi-neutron emission [21]. This is a more difficult task since the delayed neutron emission probability ( $P_n$ -value) [22] puts an additional constraint on the  $\beta$ -strength distribution in the near-threshold region.

This paper is organized as follows. In Sec. II we briefly present the modifications to the nuclear EDF which produce a SPEM, and we describe the protocol used to adjust the strength of this correction. In Sec. III, we analyze the results of the calculations of  $\beta$ -decay rates in  $^{78}\text{Ni}$  and  $^{100,132}\text{Sn}$  and the properties of the giant quadrupole resonance (GQR) and Gamow-Teller resonance (GTR) of  $^{208}\text{Pb}$ . Conclusions are drawn in Sec. IV.

## II. THE MEAN FIELD MODELS

Skyrme-type EDF are known to give an accurate description of masses and charge radii over the whole nuclear chart, from  $Z = 8$  up to heavy elements [23]. As most of the mean-field approaches, they however lead to a s.p. level density around the Fermi surface which is lower than the experimental one [9]. Here, we introduce a correction term to the Skyrme EDF which leads to a SPEM and increases the average s.p. level density [8]. We hereafter present this correction term and then briefly describe the calculations of  $\beta$ -decay rates carried out consistently in the framework of Hartree-Fock-CERPA approach.

### A. The standard Skyrme functional

The standard Skyrme functional for the time-even energy density is expressed as [23]

$$\mathcal{H}_{sky}(r) = \frac{\hbar^2}{2m}\tau_0 + \sum_{t=0,1} C_t^\rho(\rho_0)\rho_t^2 + C_t^{\Delta\rho}\rho_t\Delta\rho_t + C_t^\tau\rho_t\tau_t + \frac{1}{2}C_t^J J_t^2 + C_t^{\nabla J}\rho_t\nabla\cdot J_t, \quad (1)$$

where the indices  $t = 0, 1$  stand for the isoscalar and isovector part of the corresponding densities, respectively. For instance, the nucleonic densities  $\rho_0$  and  $\rho_1$  are defined as,

$$\begin{aligned} \rho_0(r) &= \rho_n(r) + \rho_p(r), \\ \rho_1(r) &= \rho_n(r) - \rho_p(r), \end{aligned} \quad (2)$$

where the densities  $\rho_q$  ( $q = n, p$ ) are expressed in terms of the s.p. wave functions  $\varphi_i^q$  as

$$\rho_q(r) = \sum_i |\varphi_i^q(r)|^2. \quad (3)$$

The kinetic energy and spin-current densities,  $\tau_t$  and  $J_t$ , are defined similarly [23]. The coefficients  $C_i^J$  in Eq. (1) are constants (see, e.g., Ref. [23]) except for the coefficient  $C_t^\rho$  which depends of the isoscalar density  $\rho_0$  as:

$$C_t^\rho(\rho_0) = C_t^\rho(0) + (C_t^\rho(\rho_{0,sat}) - C_t^\rho(0)) \left( \frac{\rho_0}{\rho_{0,sat}} \right)^\alpha, \quad (4)$$

where  $\rho_{0,sat}$  is the saturation density in infinite nuclear matter.

The standard Skyrme functional can be separated into neutron and proton channels, and neutron and proton effective masses are introduced:

$$\frac{m}{m_q^*} = 1 + \frac{2m}{\hbar^2} [(C_0^\tau + C_1^\tau)\rho_q + (C_0^\tau - C_1^\tau)\rho_{\bar{q}}], \quad (5)$$

Then, neutron and proton mean fields can be obtained (see appendix A).

Among the large number of Skyrme parametrizations, we have selected 6 of them based on the following requirements:

- First, the Skyrme EDF should predict  $^{132}\text{Sn}$  as a  $\beta$ -unstable nucleus at the mean field level. This is based on the common expectation that the Landau parameter  $G'_0$  in the spin-isospin channel is repulsive and will shift up the GT strength.
- Second, we wish to explore different values of effective mass in the bulk, and different isospin splittings of the effective mass.

In  $^{132}\text{Sn}$  the first condition can be related to the s.p. energy difference between the  $\pi 2d_{5/2}^5$  and  $\nu 2d_{5/2}^3$  states (which contribute mostly to the GT transition towards

TABLE I: Bulk properties of the selected interactions.

Skyrme	$\rho_{0,sat}$ (fm <sup>-3</sup> )	$E_0$ (MeV)	$K_0$ (MeV)	$J_{sym}$ (MeV)	$L_{sym}$ (MeV)	$m_s^*/m$ (MeV)	$\Delta m^*/m$	$G'_0$
SLyIII0.7 [32]	0.153	-16.33	361.4	31.98	30.78	0.7	0.18	0.30
SLyIII0.8 [32]	0.153	-16.32	368.8	31.69	28.24	0.8	0.29	0.33
SLyIII0.9 [32]	0.153	-16.31	374.5	31.44	24.75	0.9	0.38	0.34
$f_+$ [33]	0.162	-16.04	230.0	32.00	41.53	0.7	0.17	0.08
$f_0$ [33]	0.162	-16.03	230.0	32.00	42.42	0.7	0	-0.01
$f_-$ [33]	0.162	-16.02	230.0	32.00	43.79	0.7	-0.28	-0.13

the  $1^+$  state of  $^{132}\text{Sb}$ ). The lowest unperturbed transition energy is  $\epsilon_{\pi 2d\frac{5}{2}} - \epsilon_{\nu 2d\frac{3}{2}} - \Delta M_{n-H}$ , where the last term stands for the mass difference between the neutron and the hydrogen atom,  $\Delta M_{n-H} = 0.782$  MeV. If this transition energy is positive at the mean field level - hereafter called the HF transition energy - the system is  $\beta$ -stable since the CERPA correlations could only push it up, while it is expected to be actually  $\beta$ -unstable. Anticipating the discussion of the results in Sec. III we observe that models having positive HF transition energies predict  $\beta$ -decay half-lives which are too large in  $^{132}\text{Sn}$ . We therefore consider only models having a HF energy difference  $\epsilon_{\pi 2d\frac{5}{2}} - \epsilon_{\nu 2d\frac{3}{2}} < 0$ . This condition is indeed quite drastic, and we found that an appreciable number of well established Skyrme models do not fulfill it. Among these are SIII [24], BSK14-17 [25], SKM\* [24], SLy4-5 [24], SKO [26]. In addition, the models which predict that the HF transition energy is larger than 0.782 MeV are: RATP [24], SGII [27], LNS [28], LNS1, LNS5 [29], SKI1-5 [30], SAMi [31]. These models have therefore not been used here.

For the few remaining models, we restrict ourselves to the parametrizations SLyIII0.7, SLyIII0.8 and SLyIII0.9 [32] which predict in the bulk nuclear matter the effective mass values  $m^*/m=0.7, 0.8$  and  $0.9$ , respectively. We have also considered the  $f_-$ ,  $f_0$  and  $f_+$  [33] models which predict an effective mass of  $0.7$  in symmetric matter, with either a positive, zero, or negative isospin splitting of the effective mass (ISEM) in neutron matter, defined as  $m_n^*/m - m_p^*/m$ . Notice that  $m_p^*/m$  could be calculated in neutron matter without any ambiguity: the proton density shall simply be set to zero, see for instance Eq. (5).

The bulk properties of the selected interactions are given in Table I. It is observed that the saturation density  $\rho_0$ , the energy per particle at saturation  $E_0$ , and the symmetry energy  $J_{sym}$  are very similar for these interactions. The slope of the symmetry energy  $L_{sym}$  is varying between 24.75 and 43.79 MeV, which is a rather wide range, but these models are still considered as iso-soft ones. The incompressibility of SLyIII0.7, SLyIII0.8 and SLyIII0.9 is quite large. However, this does not affect the processes explored in this work. The main difference among these models comes from their effective masses

and ISEM. The models SLyIII0.7, SLyIII0.8, SLyIII0.9 have a different effective mass in symmetric matter, and a positive ISEM. The models  $f_-$ ,  $f_0$  and  $f_+$  have the same effective mass in symmetric matter and different signs for the ISEM. The models SLyIII0.7, SLyIII0.8, SLyIII0.9 and  $f_+$  have a positive ISEM, as expected from microscopic BHF and DBHF calculations [34], while  $f_0$  has no splitting and  $f_-$  has a negative ISEM. Finally, the values of the Landau parameter for the models SLyIII0.7, SLyIII0.8 and SLyIII0.9 is given by

$$G'_0 = -N_0 \left[ \frac{1}{4}t_0 + \frac{1}{24}t_3\rho^{\alpha_3} + \frac{1}{8}k_F^2(t_1 - t_2) \right] \quad (6)$$

and for the models  $f_-$ ,  $f_0$  and  $f_+$ ,

$$G'_0 = -N_0 \left[ \frac{1}{4}t_0 + \frac{1}{4}t_3\rho^{\alpha_3} + \frac{1}{4}t_4\rho^{\alpha_4} + \frac{1}{8}k_F^2(t_1 - t_2) \right] \quad (7)$$

where  $N_0 = 2k_F m^*/\pi^2 \hbar^2$  is the level density, with  $k_F$  being the Fermi momentum and  $m^*$  the nucleon effective mass. In Eq.(7), the parameter  $t_4$  is coming from an additional density-dependent term besides the usual density-dependent  $t_3$  term, and the coefficient in front of the density dependent terms have been modified w.r.t. the standard notations [33]. The values of the Landau parameter  $G'_0$  are given in the last column of Table I. At saturation density ( $\rho = \rho_0$ ), the models SLyIII0.7, SLyIII0.8, SLyIII0.9 predict rather large values for  $G'_0 \approx 0.3 - 0.35$ , while the models  $f_-$ ,  $f_0$  and  $f_+$  predict smaller value with  $G'_0 \approx 0$ . The forces  $f_-$ ,  $f_0$  and  $f_+$  clearly predict not enough positive  $G'_0$  values [19]. In addition to the different effective masses we therefore expect to observe substantial differences between these two sets of models in the charge-exchange channel.

## B. Surface-peaked effective mass correction

In Ref. [8], a surface-peaked effective mass correction to the Skyrme-type Hamiltonian was proposed with the following form,

$$\Delta \mathcal{H} = C_0^{\tau(\nabla\rho)^2} \tau (\nabla\rho)^2 + C_0^{\rho^2(\nabla\rho)^2} \rho^2 (\nabla\rho)^2, \quad (8)$$

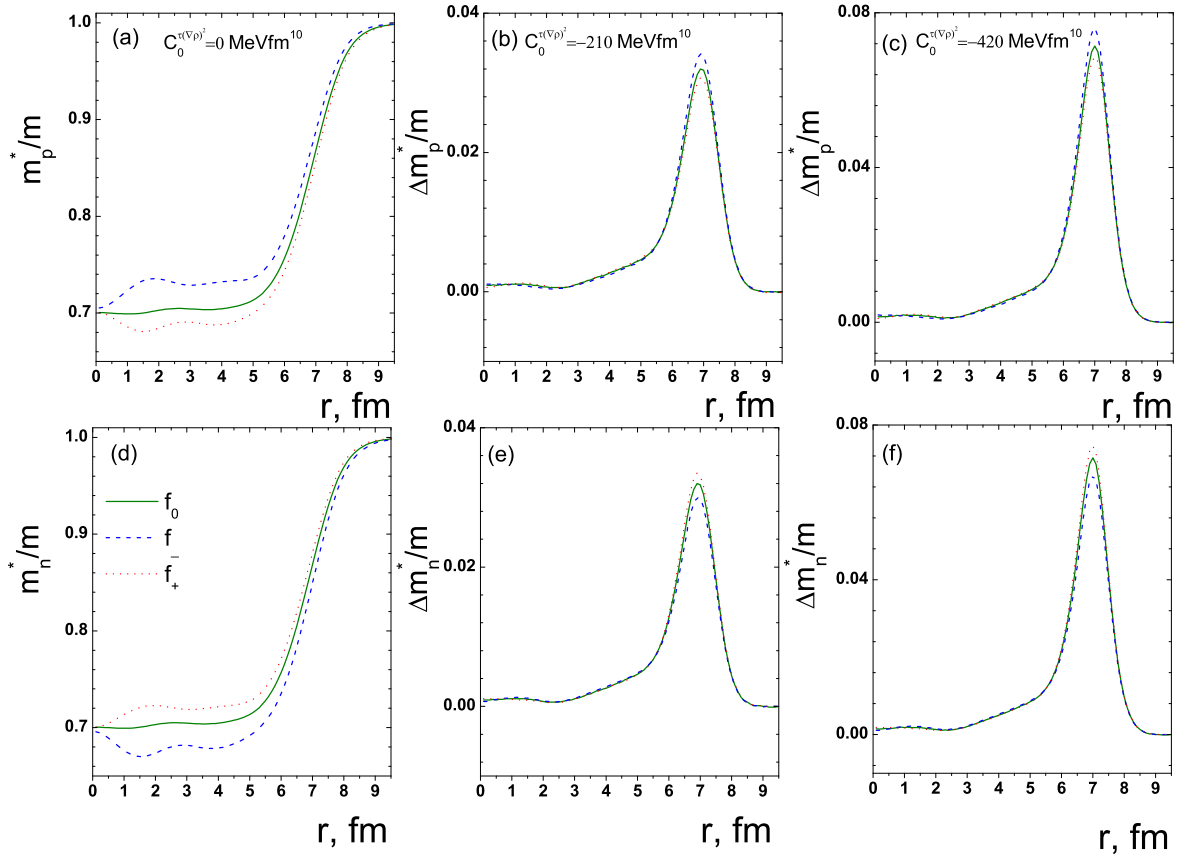


FIG. 1: (Color online) Panels (a) and (d): Proton and neutron effective masses in  $^{208}\text{Pb}$  as functions of radial distance; panels (b), (c), (e) and (f): effective-mass difference between the results of the HF calculation with the surface peaked terms ( $C_0^{\tau(\nabla\rho)^2} = -210$  MeV fm $^{10}$  and  $-420$  MeV fm $^{10}$ ), and without. Solid, dashed and dotted lines correspond to HF calculations with  $f_0$ ,  $f_-$  and  $f_+$  forces, respectively.

and the new functional can be written as  $\mathcal{H} = \mathcal{H}_{sky} + \Delta\mathcal{H}$ .

The first term of Eq.(8) is designed to modify the effective mass profile at the nuclear surface, while the second term is introduced in order to compensate the effects of the first term in the nuclear mean-field. Without the second term, the effects of the first term on the mean field are too large and drastically limit the possible values for the strength of the SPEM, as in Ref. [35]. The compensation was found to be optimal for intermediate mass and heavy nuclei if one uses the following constant relation between the two new parameters [8]:

$$C_0^{\rho^2(\nabla\rho)^2} = -10 \text{ fm } C_0^{\tau(\nabla\rho)^2}. \quad (9)$$

One can expect an impact of the SPEM on the properties of the lowest quadrupole excitation if the isoscalar terms (8) are taken into account. On the other hand, the energy-weighted sum rule (EWSR) is an integral characteristic and it is particularly sensitive to the giant-resonance properties which can be described by the EDF without the terms (8). In the present work, the values of  $C_0^{\tau(\nabla\rho)^2} = -210$  and  $-420$  MeV fm $^{10}$  are fixed so that the isoscalar quadrupole EWSR in  $^{208}\text{Pb}$  is modified by

1% and 2%, respectively. Consequently, a change of less than 0.04 of the neutron and proton effective masses at the nuclear surface of  $^{208}\text{Pb}$  is predicted, see Fig. 1. This procedure is slightly different from that used in Ref. [8], and it leads to a SPEM less strongly peaked at the surface. We have added the terms (8) without refitting the existing standard parameterizations. Using this perturbative approach, we observe a small change of the binding energies which is larger than the tolerance of the protocol for the parameter fitting. In particular, in  $^{208}\text{Pb}$  the binding energy changes by 0.35% for the SLyIII0.9 set, 0.37% for the SLyIII0.8 set, 0.38% for the SLyIII0.7 set and 0.45% for the  $f_0$ ,  $f_-$  and  $f_+$  sets. A fine tuning of other parameters in order to compensate for these energy changes has still to be done.

In Fig. 1 are shown the effective mass profiles in  $^{208}\text{Pb}$  for the  $f_0$ ,  $f_-$  and  $f_+$  models where we have considered different values of the parameter governing the strength of the SPEM,  $C_0^{\tau(\nabla\rho)^2} = 0, -210$  and  $-420$  MeV fm $^{10}$ . We remind that the differences between the models  $f_0$ ,  $f_-$  and  $f_+$  are mostly the ISEM in asymmetric matter:  $f_+$  has  $m_n^* > m_p^*$  in neutron rich matter, while  $f_-$  has  $m_n^* < m_p^*$ , and  $f_0$  has  $m_n^* = m_p^*$  in the same conditions



of isospin asymmetry. The effect of the sign difference of the effective mass splitting can also be observed on panels (a) and (d) (without SPEM): Since  $^{208}\text{Pb}$  is a neutron rich nucleus, the neutron effective mass is larger than the proton one for the  $f_+$  model, an opposite effect is found for  $f_-$ , and no effect is observed for  $f_0$ . Additionally, it is observed in panels (b), (c), (e) and (f) that the SPEM correction is almost unaffected by the effective mass splitting, since the correction is isoscalar.

### C. Calculations of $\beta$ -decay rates

We describe the collective modes in the charge-exchange random phase approximation (CERPA) using the same Skyrme interactions as above. Making use of the finite-rank separable approximation (FRSA) [36–38] for the p-h interaction enables us to perform CERPA calculations in very large configuration spaces. Although it is well known that the tensor interaction influences also the description of the  $\beta^-$ -decay half-lives [39], in the present study the tensor force is neglected in order to focus on the impact of the SPEM.

The experimentally known values of the half-lives put an indirect constraint on the calculated GT strength distributions within the  $Q_\beta$ -window. To calculate the half-lives an approximation worked out in Ref. [40] is used. It allows one to avoid an implicit calculation of the nuclear masses and  $Q_\beta$ -values. However, one should realize that the related uncertainty in constraining the parent nucleus ground state calculated with the chosen Skyrme interaction is transferred to the values of the neutron and proton chemical potentials. In the allowed GT approximation, the  $\beta^\pm$ -decay rate is expressed by summing the probabilities of the energetically allowed transitions (in units of  $G_A^2/4\pi$ ) weighted with the integrated Fermi function. For the  $\beta^-$ -decay case we have:

$$T_{1/2}^{\beta^-} = \frac{D}{\left(\frac{G_A}{G_V}\right)^2 \sum_k f_0(Z+1, A, E_i - E_{1_k^+}) B(GT)_k^-}, \quad (10)$$

$$E_i - E_{1_k^+} \approx \Delta M_{n-H} + \mu_n - \mu_p - E_k \quad (11)$$

while for the  $\beta^+$ -decay case this becomes:

$$T_{1/2}^{\beta^+} = \frac{D}{\left(\frac{G_A}{G_V}\right)^2 \sum_k f_0(-Z+1, A, E_i - E_{1_k^+}) B(GT)_k^+}, \quad (12)$$

$$E_i - E_{1_k^+} \approx -\Delta M_{n-H} - 2m_e - \mu_n + \mu_p - E_k. \quad (13)$$

Here,  $D=6147$  [41] is a constant,  $G_A/G_V=1.25$  [41] is the ratio of the weak axial-vector and vector coupling constants,  $m_e$  is the positron mass;  $\mu_n$  and  $\mu_p$  are the neutron and proton chemical potentials.  $E_i$  is the ground state energy of the parent nucleus ( $Z, A$ ) and  $E_{1_k^+}$  denotes a state of the daughter nucleus. The  $E_k$  are the  $1^+$

TABLE II: Energy differences between the dominant s.p. states in  $^{132}\text{Sn}$  and  $^{100}\text{Sn}$ . For each Skyrme parameterization, the energy difference is calculated with the surface peaked term or without ( $C_0^{\tau(\nabla\rho)^2} = 0$ ). See text for more details.

Skyrme	$C_0^{\tau(\nabla\rho)^2}$ (MeV fm <sup>10</sup> )	$^{132}\text{Sn}$	$^{100}\text{Sn}$	$^{78}\text{Ni}$
		$\epsilon_{\pi 2d \frac{5}{2}} - \epsilon_{\nu 2d \frac{3}{2}}$ (MeV)	$\epsilon_{\nu 1g \frac{7}{2}} - \epsilon_{\pi 1g \frac{9}{2}}$ (MeV)	$\epsilon_{\pi 2p \frac{3}{2}} - \epsilon_{\nu 2p \frac{1}{2}}$ (MeV)
SLyIII0.7	0	0.3	-7.2	-5.1
SLyIII0.7	-210	0.2	-7.3	-5.2
SLyIII0.7	-420	0.1	-7.3	-5.3
SLyIII0.8	0	-0.6	-7.5	-6.2
SLyIII0.8	-210	-0.7	-7.5	-6.3
SLyIII0.8	-420	-0.9	-7.6	-6.4
SLyIII0.9	0	-1.3	-7.7	-7.0
SLyIII0.9	-210	-1.4	-7.7	-7.2
SLyIII0.9	-420	-1.6	-7.8	-7.3
$f_+$	0	-0.6	-5.9	-5.8
$f_+$	-210	-0.7	-6.0	-5.9
$f_+$	-420	-0.8	-6.2	-6.0
$f_0$	0	-0.5	-6.0	-5.6
$f_0$	-210	-0.6	-6.1	-5.7
$f_0$	-420	-0.7	-6.2	-5.8
$f_-$	0	-0.4	-6.2	-5.4
$f_-$	-210	-0.5	-6.3	-5.5
$f_-$	-420	-0.6	-6.5	-5.6

eigenvalues of the CERPA equations. The CERPA wave functions allow us to determine GT transitions whose operator is  $\hat{O}_\pm = \sum_{i,m} t_\pm(i) \sigma_m(i)$ .

$$B(GT)_k^\pm = \left| \langle N \pm 1, Z \mp 1; 1_k^+ | \hat{O}^\pm | N, Z; 0_{gs}^+ \rangle \right|^2. \quad (14)$$

Expressions (10)-(14) will be used in the next section to calculate the  $\beta$ -decay rates and the collective modes. All the calculations are performed without any quenching factor.

### III. RESULTS FOR COLLECTIVE MODES AND $\beta$ -DECAY RATES

We now analyze first the results of the  $\beta$ -decay rates which are sensitive to the low-energy part of the CERPA strength, and then the GT collective modes. The effects of the SPEM will be discussed.

The p-h interaction in the spin-isospin channel is assumed of the following form:

$$V(\mathbf{r}_1, \mathbf{r}_2) = N_0^{-1} G_0'(r_1) \boldsymbol{\sigma}^{(1)} \cdot \boldsymbol{\sigma}^{(2)} \boldsymbol{\tau}^{(1)} \cdot \boldsymbol{\tau}^{(2)} \delta(\mathbf{r}_1 - \mathbf{r}_2) \quad (15)$$

where  $\boldsymbol{\sigma}^{(i)}$  and  $\boldsymbol{\tau}^{(i)}$  are the spin and isospin operators. As expected, the largest contribution to the calculated

TABLE III: SPEM effects on  $\beta^-$ -decay properties of  $^{132}\text{Sn}$ . Data are from Ref. [43].

Skyrme	$C_0^{\tau(\nabla\rho)^2}$ (MeV fm <sup>10</sup> )	$E_i - E_{1^+}$ (MeV)	$B(GT)_1^-$	$T_{1/2}$ (s)
SLyIII0.7	0	0.07	2.6	389400
SLyIII0.7	-210	0.21	2.7	9840
SLyIII0.7	-420	0.34	2.7	1930
SLyIII0.8	0	0.97	2.5	57
SLyIII0.8	-210	1.11	2.5	33
SLyIII0.8	-420	1.26	2.6	21
SLyIII0.9	0	1.70	2.4	6.7
SLyIII0.9	-210	1.84	2.5	4.7
SLyIII0.9	-420	2.01	2.6	3.3
$f_+$	0	1.12	4.6	18
$f_+$	-210	1.25	4.6	12
$f_+$	-420	1.36	4.6	8.5
$f_0$	0	1.14	5.9	13
$f_0$	-210	1.27	5.8	8.8
$f_0$	-420	1.37	5.8	6.5
$f_-$	0	1.12	8.8	6.4
$f_-$	-210	1.25	8.7	5.0
$f_-$	-420	1.36	8.6	3.6
Expt.		1.794±0.009		39.7±0.8

TABLE IV: SPEM effects on  $\beta^-$ -decay properties of  $^{78}\text{Ni}$ . Data are from Refs. [44].

Skyrme	$C_0^{\tau(\nabla\rho)^2}$ (MeV fm <sup>10</sup> )	$E_i - E_{1^+}$ (MeV)	$B(GT)_1^-$	$T_{1/2}$ (s)
SLyIII0.7	0	5.49	1.0	0.157
SLyIII0.7	-210	5.61	1.1	0.140
SLyIII0.7	-420	5.74	1.1	0.121
SLyIII0.8	0	6.60	1.0	0.057
SLyIII0.8	-210	6.73	1.0	0.051
SLyIII0.8	-420	6.87	1.0	0.045
SLyIII0.9	0	7.48	1.0	0.025
SLyIII0.9	-210	7.61	1.0	0.023
SLyIII0.9	-420	7.79	1.0	0.020
$f_+$	0	6.40	1.9	0.031
$f_+$	-210	6.51	1.9	0.028
$f_+$	-420	6.60	1.9	0.027
$f_0$	0	6.33	2.6	0.020
$f_0$	-210	6.44	2.5	0.019
$f_0$	-420	6.52	2.5	0.018
$f_-$	0	6.33	3.9	0.010
$f_-$	-210	6.42	3.9	0.009
$f_-$	-420	6.50	3.8	0.009
Expt.				0.1222±0.0051

$\beta^\pm$ -decay half-life comes from the  $1_1^+$  state, the structure of which is dominated by one unperturbed configuration. They are the 1p-1h configurations  $\{\pi 2d_{5/2}^5, \nu 2d_{3/2}^3\}$ ,  $\{\nu 1g_{7/2}^7, \pi 1g_{9/2}^9\}$  and  $\{\pi 2p_{3/2}^3, \nu 2p_{1/2}^1\}$  of  $^{132}\text{Sn}$ ,  $^{100}\text{Sn}$  and  $^{78}\text{Ni}$ , respectively. In other words, the  $1_1^+$  state is non-collective and, therefore, the  $\beta$ -decay is related to the lowest unperturbed  $1^+$  energy. We first examine the s.p. energy differences given in Table II for the selected Skyrme models and for various strength of the SPEM parameter  $C_0^{\tau(\nabla\rho)^2}$ . They are small (about 1 MeV) in  $^{132}\text{Sn}$  but rather large in  $^{78}\text{Ni}$  and  $^{100}\text{Sn}$  (5 to 8 MeV). In  $^{100}\text{Sn}$ , the energy differences without SPEM are mostly sensitive to the Coulomb component of the EDF, with a small additional effect due to the effective mass (the larger effective mass, the smaller the energy difference). In  $^{132}\text{Sn}$ , the energy difference is related mostly to the symmetry energy: the larger the symmetry energy, going from SLyIII0.9 to SLyIII0.7 for instance, the larger the energy difference. In addition, the increase of the effective mass also contributes, with a smaller impact, to the decrease the energy difference, as it can be deduced from the comparison of the energy difference for the forces  $f_-$ ,  $f_0$ , and  $f_+$  which has increasing effective mass in neutron rich matter, see Fig. 1. It can be seen (cf. Table II) that the shifts in the energy differences between the cases without, and with maximal SPEM ( $C_0^{\tau(\nabla\rho)^2} = -420$  MeV fm<sup>10</sup>) are almost constant and independent of the models considered. It varies by about 0.3 MeV in  $^{132}\text{Sn}$  and in  $^{78}\text{Ni}$ . From Table II, we can anticipate that the SPEM will have a larger impact on the calculation of the  $\beta$  half-life of  $^{132}\text{Sn}$  and a weaker one in the case of  $^{78}\text{Ni}$  and  $^{100}\text{Sn}$ . In  $^{132}\text{Sn}$ , the experimental value is -1.305 MeV [42]. No data exist for  $^{78}\text{Ni}$  and  $^{100}\text{Sn}$ .

The  $E_i - E_{1^+}$  energies, the  $B(GT)_1^-$  values and  $\beta^-$ -decay half-lives of  $^{132}\text{Sn}$  and  $^{78}\text{Ni}$  are given in Tables III and IV, the  $\beta^+$ -decay properties of  $^{100}\text{Sn}$  in Table V. The evolution of the transition energies and the  $B(GT)_1^\pm$  values is reflected in the half-life behaviour, see Eqs.(10) and (12). As in Table II, the results shown in Tables III, IV and V correspond to the selected interactions with and without the SPEM represented by the value of the parameter  $C_0^{\tau(\nabla\rho)^2}$ . In the case of  $^{132}\text{Sn}$ , the model SLyIII0.7 predicts positive energy differences for the dominant transition of the  $\beta$ -decay half-lives (see Table II), and it leads to half-lives which are much larger than the experimental value, as anticipated.

One can see from Tables III, IV and V that the  $\beta$ -decay half-lives are much more sensitive to the effective mass distribution in the case of the low- $Q_\beta$  nucleus  $^{132}\text{Sn}$  than in  $^{100}\text{Sn}$  and  $^{78}\text{Ni}$ . For  $^{132}\text{Sn}$ , a strong decrease of the half-life can be directly correlated to either the increase of the effective mass in symmetric matter, or to the increase of the SPEM, while in  $^{78}\text{Ni}$  and  $^{100}\text{Sn}$ , the correlation, while still being present, is much less pronounced. This can be easily understood from the energy difference of the most important transition given in Table II: The energy differences are much smaller in the case of  $^{132}\text{Sn}$  than

TABLE V: SPEM effects on  $\beta^+$ -decay properties of  $^{100}\text{Sn}$ . Data are from Ref. [45].

Skyrme	$C_0^{\tau(\nabla\rho)^2}$ (MeV fm <sup>10</sup> )	$E_i - E_{1^+}$ (MeV)	$B(GT)_1^+$	$T_{1/2}$ (s)
SLyIII0.7	0	4.26	15.2	0.232
SLyIII0.7	-210	4.38	15.2	0.221
SLyIII0.7	-420	4.42	15.2	0.213
SLyIII0.8	0	4.60	15.1	0.178
SLyIII0.8	-210	4.64	15.1	0.172
SLyIII0.8	-420	4.67	15.0	0.167
SLyIII0.9	0	4.86	15.1	0.138
SLyIII0.9	-210	4.90	15.0	0.134
SLyIII0.9	-420	4.92	15.0	0.131
$f_+$	0	3.47	16.3	0.593
$f_+$	-210	3.62	16.3	0.492
$f_+$	-420	3.72	16.2	0.433
$f_0$	0	3.80	16.8	0.381
$f_0$	-210	3.94	16.8	0.323
$f_0$	-420	4.04	16.7	0.290
$f_-$	0	4.38	17.6	0.190
$f_-$	-210	4.51	17.5	0.168
$f_-$	-420	4.60	17.5	0.154
Expt.		$3.08 \pm 0.34$		$1.16 \pm 0.20$

TABLE VI: SPEM effects on the energy and  $B(E2)$ -value for the up-transition to the first  $2^+$  state in  $^{208}\text{Pb}$ . Data are from Ref. [43].

Skyrme	$C_0^{\tau(\nabla\rho)^2}$ (MeV fm <sup>10</sup> )	Energy (MeV)	$B(E2; 0_{gs}^+ \rightarrow 2_1^+)$ (e <sup>2</sup> fm <sup>4</sup> )
$f_+$	0	5.12	3130
$f_+$	-210	5.09	2530
$f_+$	-420	5.09	2180
$f_0$	0	5.13	3250
$f_0$	-210	5.09	2650
$f_0$	-420	5.09	2310
$f_-$	0	5.09	3440
$f_-$	-210	5.06	2850
$f_-$	-420	5.06	2500
Expt.		4.09	$3000 \pm 300$

in the case of  $^{100}\text{Sn}$  and  $^{78}\text{Ni}$ , which makes the  $\beta$ -decay half-lives more sensitive to a small modification of the s.p. energies induced by the SPEM.

Let us examine whether the SPEM could improve the agreement between the model predictions and the experimental values. As one can see from Tables III, IV and V the inclusion of the terms (8) leads to minor effects on the  $B(GT)_1^+$  values. We find that the SPEM induces an increase of the transition energies and it results in a

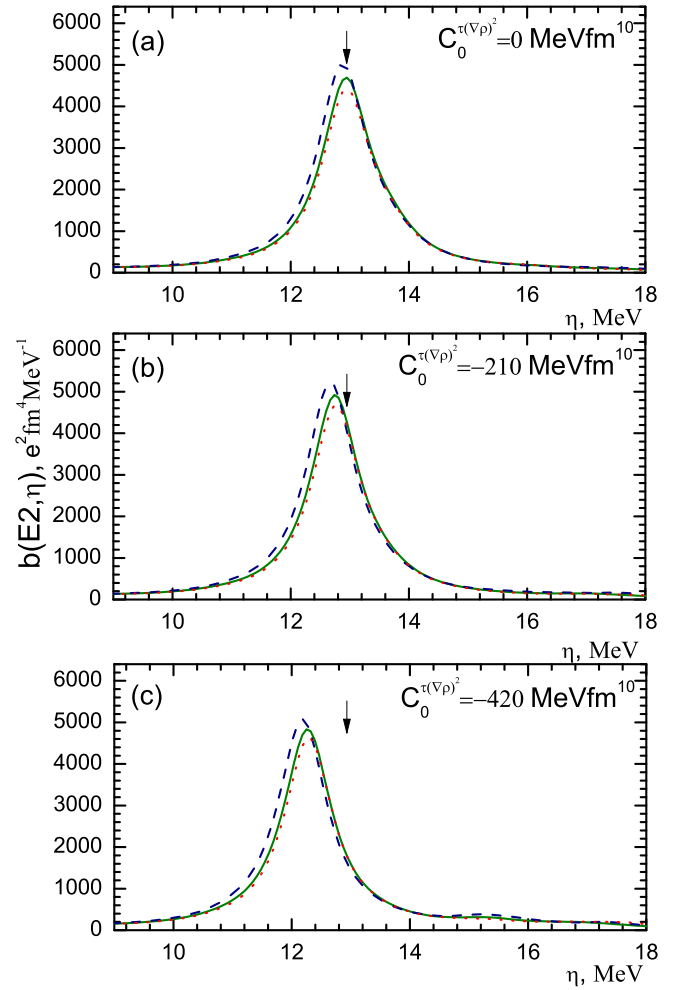


FIG. 2: (Color online) The quadrupole strength distribution of  $^{208}\text{Pb}$ . Solid, dashed and dotted lines correspond to RPA calculations with  $f_0$ ,  $f_-$  and  $f_+$  models, respectively. The experimental centroid of the GQR is at  $10.89 \pm 0.30$  MeV [46].

decrease of the half-lives. We first concentrate on the models SLyIII0.7, SLyIII0.8 and SLyIII0.9, which correspond to different values of the effective mass in symmetric matter. From the comparison of the theoretical predictions with the experimental half-lives shown in Tables III, IV and V, it is difficult to conclude which model is better: For  $^{132}\text{Sn}$ , the model SLyIII0.8 is preferred, for  $^{78}\text{Ni}$  and  $^{100}\text{Sn}$ , it is SLyIII0.7. Now, if we concentrate on the models  $f_+$ ,  $f_0$  and  $f_-$ , it is  $f_+$  which always comes the closest to the experimental value. This indicates that, in addition to the effective mass, the residual interaction is very important. It was already anticipated that the value of the Landau parameter  $G'_0$  for the selected models (cf. Table I) could have an impact on charge-exchange related observables. For the models  $f_+$ ,  $f_0$  and  $f_-$  the values of  $G'_0$  are too small. Since the impact of the SPEM on the  $\beta$ -decay rates in  $^{78}\text{Ni}$  and  $^{100}\text{Sn}$  is quite small, these nuclei could be, in the future, used to calibrate the residual interaction almost independently from the profile of the



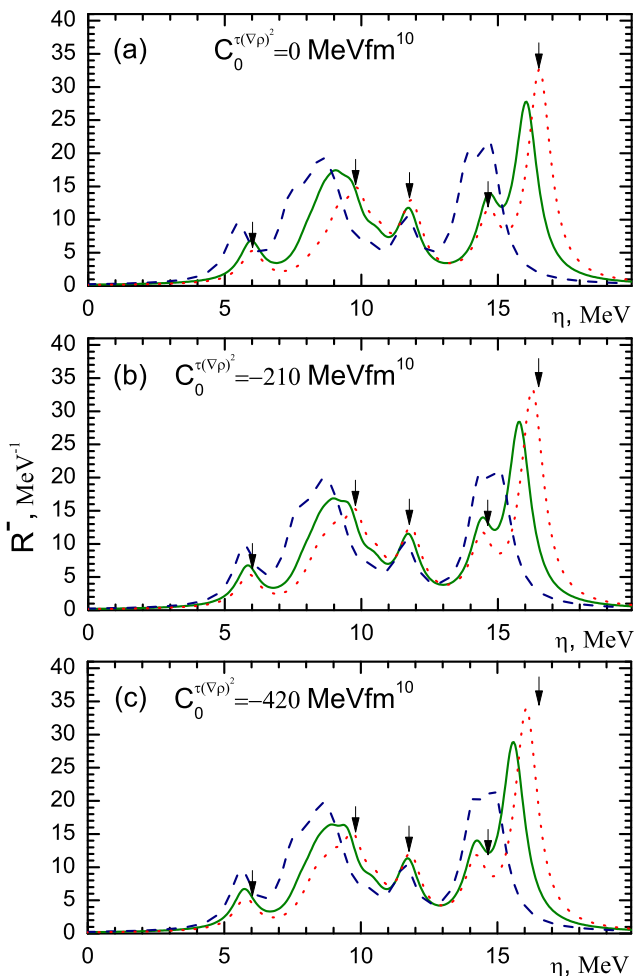


FIG. 3: (Color online) Same as Fig. 2, for the GT strength distribution obtained within the CERPA. The experimental centroids of the GTR is at 19.2 MeV [47, 48].

effective mass. The modification of  $G'_0$  could be obtained from a refitting of the Skyrme functional with a different value of the strength of the SPEM. One could increase  $G'_0$  by about 0.1-0.2 by introducing the spin-density dependent extension of the Skyrme model [49, 50]. This will be left for future investigations.

Up to this point, we have mostly focused on the relation between the SPEM and the low energy part of the strength, since it represents the main contribution to the  $\beta$ -decay rates. We now turn to the higher energy part and show in Figs. 2 and 3 the effects of the SPEM on the properties of the GQR and GTR in  $^{208}\text{Pb}$ . In the figures, the calculated strength distributions are folded out with a Lorentzian distribution of 1 MeV width. The excitation energies refer to the ground state of the parent nucleus  $^{208}\text{Pb}$ . The arrows indicate the maxima of the strength distributions corresponding to the case of the  $f_+$  model and  $C_0^{\tau(\nabla\rho)^2}=0 \text{ MeV fm}^{10}$ . Since the isoscalar quadrupole EWSR is changed by only about 1% by the SPEM, we expect the collective modes at higher energy

to be only marginally impacted.

The GQR strength distribution consists mostly of a main peak. Comparing the cases without SPEM and with maximal SPEM, we find that the peak is shifted down by about 500 keV. One can notice that the GQR strength distribution is almost identical for the three models  $f_0$ ,  $f_+$  and  $f_-$ . As can be seen from Table VI, while the  $2_1^+$  energy is practically unaffected by the SPEM, the  $B(E2)$  value is decreasing as the SPEM increases. Some overestimate of the experimental energy indicates that there is room for the two-phonon effects [51].

The GTR is much more fragmented than the GQR, as seen in Fig. 3. The strength distribution is globally shifted up as the isospin splitting is going from positive ( $f_+$ ) to negative values ( $f_-$ ). As in the case of the GQR, the high energy peaks of the strength distribution are shifted to lower energies (by about 500 keV) as the SPEM gets larger. This is an effect of the slight increase of the level density induced by the SPEM.

#### IV. CONCLUSIONS

Starting from different Skyrme EDF which predict  $^{132}\text{Sn}$   $\beta$ -unstable, we have studied the effects of introducing a surface-peaked effective mass on top of existing Skyrme models. The main effect of this additional term is a compression of the s.p. level spacing around the Fermi level, or equivalently, an increase of the level density. This systematically increases the  $\beta$ -decay rates (i.e., decreases the half-lives). The collective modes at higher energy are only slightly impacted by the SPEM.

This work is a first step towards improving Skyrme functionals by adding extra terms to the energy functional. Our motivation is based on both having a better agreement with nuclear data, and also predicting weak transition rates for astrophysical applications. The results of our analysis allow for a better understanding of the effects at play. The  $\beta$ -decay rates in doubly-magic unstable nuclei ( $^{100,132}\text{Sn}$ ,  $^{78}\text{Ni}$ ) are indeed very sensitive both to the s.p. energies and residual interactions, and none of the Skyrme models selected in this work are fully satisfactory in this respect. From our analysis, we have however identified two nuclei ( $^{100}\text{Sn}$ ,  $^{78}\text{Ni}$ ) where the  $\beta$ -decay half-lives are only weakly impacted by the SPEM. They can be considered as good benchmark nuclei since they potentially offer the possibility to calibrate the residual interaction, with a weak influence of the effective mass. In a complementary approach,  $^{132}\text{Sn}$  could be used to test different strengths of the SPEM, for a fixed residual interaction.

The tensor force has not been considered in this work, although it can affect the neutron-proton s.p. energies in some cases. We have aimed at understanding just the contribution of the SPEM to the  $\beta$ -decay and GT mode in order to disentangle the respective roles of the effective mass and the residual interaction. An additional

modification of the Skyrme functional was proposed earlier in order to stabilize the nuclear matter equation of state [49, 50]. It has been recently used in nuclei and, since it brings an additional repulsive term to the  $G'_0$  Landau parameter, it was shown to shift the centroids of the GT collective mode to higher energies by a few hundreds keV up to 1 MeV [52]. In the future, we plan to explore the predictions of a general mean field model including all these ingredients, and to compare them to known experimental data, as done in this work. These calibration processes are important to set-up boundaries for the additional parameters before making predictions for astrophysical cases.

### Acknowledgments

A.P.S. and I.N.B. thank the hospitality of IPN-Orsay and IPN-Lyon where a part of this work was done. This work is partly supported by the IN2P3-JINR agreement and the ANR project "SN2NS: supernova explosions, from stellar core-collapse to neutron stars and black holes".

### Appendix A: Decomposition of the Skyrme functional into neutron and proton channels

Here, the Skyrme functional is expressed in terms of the neutron and proton densities instead of the isoscalar and isovector densities,

$$\mathcal{H}_{sky}(r) = \sum_{q=n,p} h_q^\rho + h_q^\nabla + h_q^J, \quad (\text{A1})$$

where the different terms of the energy density are

$$h_q^\rho = \frac{\hbar^2}{2m} f_q^{\text{Sky}} \tau_q + (C_0^\rho + C_1^\rho) \rho_q^2 + (C_0^\rho - C_1^\rho) \rho_q \rho_{\bar{q}} \quad (\text{A2})$$

$$h_q^\nabla = -(C_0^{\Delta\rho} + C_1^{\Delta\rho})(\nabla\rho_q)^2 - (C_0^{\Delta\rho} - C_1^{\Delta\rho})\nabla\rho_q \cdot \nabla\rho_{\bar{q}} \quad (\text{A3})$$

$$h_q^J = \frac{1}{2}(C_0^J + C_1^J)J_q^2 + \frac{1}{2}(C_0^J - C_1^J)J_q J_{\bar{q}} - [(C_0^{\nabla J} + C_1^{\nabla J})\nabla\rho_q + (C_0^{\nabla J} - C_1^{\nabla J})\nabla\rho_{\bar{q}}] \cdot J_q, \quad (\text{A4})$$

and the effective mass factor  $f_q^{\text{Sky}} = m/m_q^*$  is defined as

$$f_q^{\text{Sky}} = 1 + \frac{2m}{\hbar^2} [(C_0^\tau + C_1^\tau)\rho_q + (C_0^\tau - C_1^\tau)\rho_{\bar{q}}]. \quad (\text{A5})$$

By functional derivation the one-body Hamiltonian  $\mathcal{H}_q$  is obtained as,

$$\mathcal{H}_q = -\frac{\hbar^2}{2m} \nabla \cdot f_q^{\text{Sky}}(r) \nabla + V_q(r) - \frac{i}{2} \sum_{\sigma'} [W_q \cdot (\nabla \times \langle \sigma | \sigma' \rangle) + (\nabla \times \langle \sigma | \sigma' \rangle) \cdot W_q] \quad (\text{A6})$$

where the central potential is given by

$$V_q^{\text{Sky}}(r) = V_q^\rho(r) + V_q^\nabla(r) + V_q^J(r). \quad (\text{A7})$$

Here, the central-density potential is given by:

$$V_q^\rho(r) = (C_0^\tau + C_1^\tau)\tau_q + (C_0^\tau - C_1^\tau)\tau_{\bar{q}} + 2[(C_0^\rho + C_1^\rho)\rho_q + (C_0^\rho - C_1^\rho)\rho_{\bar{q}}] + \frac{\partial}{\partial\rho_0}(C_0^\rho + C_1^\rho)\rho_q^2 + \frac{\partial}{\partial\rho_0}(C_0^\rho - C_1^\rho)\rho_q\rho_{\bar{q}}, \quad (\text{A8})$$

the central-gradient potential by:

$$V_q^\nabla(r) = 2(C_0^{\Delta\rho} + C_1^{\Delta\rho})\nabla^2\rho_q + 2(C_0^{\Delta\rho} - C_1^{\Delta\rho})\nabla^2\rho_{\bar{q}}, \quad (\text{A9})$$

and the central- $J$  potential by:

$$V_q^J(r) = (C_0^{\nabla J} + C_1^{\nabla J})\nabla \cdot J_q + (C_0^{\nabla J} - C_1^{\nabla J})\nabla \cdot J_{\bar{q}}. \quad (\text{A10})$$

The spin-orbit potential is:

$$W_q(r) = -(C_0^{\nabla J} + C_1^{\nabla J})\nabla\rho_q - (C_0^{\nabla J} - C_1^{\nabla J})\nabla\rho_{\bar{q}} + (C_0^J + C_1^J)J_q + (C_0^J - C_1^J)J_{\bar{q}}. \quad (\text{A11})$$

### Appendix B: Modification of the mean-field equations induced by the SPEM

The kinetic energy correction induced by the effective mass in Eq. (A2) is now given by  $f_q = f_q^{\text{Sky}} + f_q^{\text{corr}}$  where

$$f_q^{\text{corr}} = \frac{2m}{\hbar^2} C_0^{\tau(\nabla\rho)^2} (\nabla\rho(\mathbf{r}))^2, \quad (\text{B1})$$

and the mean field central potential (A7) reads:

$$V_q(\mathbf{r}) = V_q^{\text{Sky}}(\mathbf{r}) + V_q^{\text{corr}}(\mathbf{r}), \quad (\text{B2})$$

where  $V_q^{\text{Sky}}(\mathbf{r})$  is the mean field deduced from the Skyrme interaction, e.g. Eq. (A7), and  $V_q^{\text{corr}}(\mathbf{r})$  is the correction term induced by Eq. (8):

$$V_q^{\text{corr}}(\mathbf{r}) = -2C_0^{\tau(\nabla\rho)^2} \left( \tau(\mathbf{r})\nabla^2\rho(\mathbf{r}) + \nabla\tau(\mathbf{r})\nabla\rho(\mathbf{r}) \right) - 2C_0^{\rho^2(\nabla\rho)^2} \left( \rho(\mathbf{r})(\nabla\rho(\mathbf{r}))^2 + \rho(\mathbf{r})^2\nabla^2\rho(\mathbf{r}) \right). \quad (\text{B3})$$

- 
- [1] H. A. Bethe, Rev. Mod. Phys. **62**, 801 (1990).
- [2] K. Langanke and G. Martínez-Pinedo, Rev. Mod. Phys. **75**, 819 (2003).
- [3] K. Langanke and G. Martínez-Pinedo, Nucl. Phys. A **673**, 481 (2000); *ibid.*, At. Data Nucl. Data Tables **79**, 1 (2001).
- [4] G. Martínez-Pinedo, K. Langanke, and D.J. Dean, Astrophys. J. Suppl. Ser. **126**, 493 (2000).
- [5] N. Paar, G. Colò, E. Khan, and D. Vretenar, Phys. Rev. C **80**, 055801 (2009).
- [6] Y. F. Niu, N. Paar, D. Vretenar, and J. Meng, Phys. Rev. C **83**, 045807 (2011).
- [7] A. F. Fantina, E. Khan, G. Colò, N. Paar, and D. Vretenar, Phys. Rev. C **86**, 035805 (2012).
- [8] A. F. Fantina, J. Margueron, P. Donati, P. M. Piz-zochero, J. Phys. G **38**, 025101 (2011).
- [9] G. E. Brown, J. H. Guun, and P. Gould, Nucl. Phys. **46**, 598 (1964).
- [10] M. N. Harakeh, and A. Van der Woude, Giant Resonances: Fundamental High-Frequency Modes of Nuclear Excitation. Oxford Studies in Nuclear Physics (New-York: Oxford University Press) (2001).
- [11] J.P. Jeukenne, A. Lejeune, and C. Mahaux, Phys. Reports **25**, 83 (1976).
- [12] C. Mahaux and R. Sartor, Adv. Nucl. Phys. (Springer Verlag Ed.), p. 1-223 (1991).
- [13] N. Vinh Mau and A. Bouyssy, Nucl. Phys. A **257**, 189 (1976).
- [14] V. Bernard and Nguyen Van Giai, Nucl. Phys. A **348**, 75 (1980).
- [15] L.G. Cao, G. Colò, H. Sagawa, and P.F. Bortignon, arXiv:1401.1983.
- [16] Z. Y. Ma and J. Wambach, Nucl. Phys. A **402**, 275 (1983).
- [17] E. V. Litvinova and A. V. Afanasjev, Phys. Rev. C **84**, 014305 (2011).
- [18] M. Farine, J.M. Pearson, and F. Tondeur, Nucl. Phys. A **696**, 396 (2001).
- [19] I.N. Borzov, Nucl. Phys. A **777**, 645 (2006).
- [20] P. T. Hosmer, H. Schatz, A. Aprahamian, O. Arndt, R. R. C. Clement, A. Estrade, K.-L. Kratz, S. N. Liddick, P. F. Mantica, W. F. Mueller, F. Montes, A. C. Morton, M. Ouellette, E. Pellegrini, B. Pfeiffer, P. Reeder, P. Santi, M. Steiner, A. Stolz, B. E. Tomlin, W. B. Walters, and A. Wöhr, Phys. Rev. Lett. **94**, 112501 (2005).
- [21] K. Miernik, K. P. Rykaczewski, C. J. Gross, R. Grzywacz, M. Madurga, D. Miller, J. C. Batchelder, I. N. Borzov, N. T. Brewer, C. Jost, A. Korgul, C. Mazzocchi, A. J. Mendez, Y. Liu, S.V. Paulauskas, D.W. Stracener, J. A. Winger, M. Wolińska-Cichocka, and E. F. Zganjar, Phys. Rev. Lett. **111**, 132502 (2013).
- [22] I.N. Borzov, Phys. Rev. C **71**, 065801 (2005).
- [23] M. Bender, P.-H. Heenen, and P.-G. Reinhard, Rev. Mod. Phys. **75**, 121180 (2003).
- [24] E. Chabanat, P. Bonche, P. Haensel, J. Meyer, and R. Schaeffer, Nucl. Phys. A **627**, 710 (1997).
- [25] S. Goriely, N. Chamel, and J. M. Pearson, Phys. Rev. Lett. **102**, 152503 (2009).
- [26] P.-G. Reinhard, D. J. Dean, W. Nazarewicz, J. Dobaczewski, J. A. Maruhn, and M. R. Strayer, Phys. Rev. C **60**, 014316 (1999).
- [27] Nguyen Van Giai and H. Sagawa, Phys. Lett. **B106**, 379 (1981).
- [28] L. G. Cao, U. Lombardo, C.W. Shen, and N. Van Giai, Phys. Rev. C **73**, 014313 (2006).
- [29] D. Gambacurta, L. Li, G. Colò, U. Lombardo, N. Van Giai, and W. Zuo, Phys. Rev. C **84**, 024301 (2011).
- [30] P.-G. Reinhard and H. Flocard, Nucl. Phys. A **584**, 467 (1995).
- [31] X. Roca-Maza, G. Colò, and H. Sagawa, Phys. Rev. C **86**, 031306 (2012).
- [32] K. Washiyama, K. Bennaceur, B. Avez, M. Bender, P.-H. Heenen, and V. Hellemaans, Phys. Rev. C **86**, 054309 (2012).
- [33] T. Lesinski, K. Bennaceur, T. Duguet, and J. Meyer, Phys. Rev. C **74**, 044315 (2006).
- [34] E. N. E. van Dalen, C. Fuchs, and A. Faessler, Phys. Rev. Lett. **95**, 022302 (2005).
- [35] M. Zalewski, P. Olbratowski, and W. Satula, Int. J. Mod. Phys. E **19**, 794 (2010) ; *ibid.*, Phys. Rev. C **81**, 044314 (2010).
- [36] Nguyen Van Giai, Ch. Stoyanov, and V. V. Voronov, Phys. Rev. C **57**, 1204 (1998).
- [37] A. P. Severyukhin, V. V. Voronov, and Nguyen Van Giai, Phys. Rev. C **77**, 024322 (2008).
- [38] A. P. Severyukhin, V. V. Voronov, and Nguyen Van Giai, Prog. Theor. Phys. **128**, 489 (2012).
- [39] F. Minato and C. L. Bai, Phys. Rev. Lett. **110**, 122501 (2013).
- [40] J. Engel, M. Bender, J. Dobaczewski, W. Nazarewicz, and R. Surman, Phys. Rev. C **60**, 014302 (1999).
- [41] J. Suhonen, *From Nucleons to Nucleus* (Springer-Verlag, Berlin, 2007).
- [42] K.A. Mezilev, Y.N. Novikov, V.A. Popov, B. Fogelberg, and L. Spanier, Phys. Scr. **T56**, 227 (1995).
- [43] National Nuclear Data Center, <http://www.nndc.bnl.gov>.
- [44] Z. Y. Xu, S. Nishimura, G. Lorusso, F. Browne, P. Doornenbal, G. Gey, H.-S. Jung, Z. Li, M. Niikura, P.-A. Söderström, T. Sumikama, J. Taprogge, Zs. Vajta, H. Watanabe, J. Wu, A. Yagi, K. Yoshinaga, H. Baba, S. Franchoo, T. Isobe, P. R. John, I. Kojouharov, S. Kubono, N. Kurz, I. Matea, K. Matsui, D. Mengoni, P. Morfouace, D. R. Napoli, F. Naqvi, H. Nishibata, A. Odahara, E. Şahin, H. Sakurai, H. Schaffner, I. G. Stefan, D. Suzuki, R. Taniuchi, and V. Werner, Phys. Rev. Lett. **113**, 032505 (2014).
- [45] C. B. Hinke et al., Nature **486**, 341 (2012).
- [46] D. H. Youngblood, Y.-W. Lui, H. L. Clark, B. John, Y. Tokimoto, and X. Chen, Phys. Rev. C **69**, 034315 (2004).
- [47] D. J. Horen, C. D. Goodman, C. C. Foster, C. A. Goulding, M. B. Greenfield, J. Rapaport, and D.E. Bainum, Phys. Lett. B **95**, 27 (1980).
- [48] A. Krasznahorkay, H. Akimune, M. Fujiwara, M. N. Harakeh, J. Jänecke, V. A. Rodin, M. H. Urin, and M. Yosoi, Phys. Rev. C **64**, 067302 (2001).
- [49] J. Margueron, S. Goriely, M. Grasso, G. Colò, and H. Sagawa, Journ. Phys. G **36**, 125103 (2009).
- [50] J. Margueron and H. Sagawa, Journ. Phys. G **36**, 125102 (2009).
- [51] A. P. Severyukhin, V. V. Voronov, and Nguyen Van Giai, Eur. Phys. J. **A22**, 397 (2004).

- [52] P. Wen, L.-G. Cao, J. Margueron and H. Sagawa, Phys. Rev. C 89, 044311 (2014)